ECS Transactions, 80 (10) 621-633 (2017)
10.1149/08010.0621ecst ©The Electrochemical Society

Correlation between electrical properties of the passive film on carbon steel and inhibition efficiency by phosphate and nitrite ions

M.A. Frontini, M. Vázquez and M. B. Valcarce

División Electroquímica Aplicada,
Facultad de Ingeniería, Universidad Nacional de Mar del Plata
INTEMA, CONICET, J. B. Justo 4302, B7608FDQ Mar del Plata, ARGENTINA

The electronic properties of passive films grown at open circuit potential for 24 h and 7 days in pore simulating solutions are correlated to the inhibiting effect of nitrite and phosphate ions in chloride-rich alkaline solutions. Electrochemical impedance and Mott-Schottky plots were used to investigate the electronic properties of the films grown. Changes in composition were analyzed by X-ray photoelectron spectroscopy.
Both anions are excellent inhibitors. However, the donor density (N_D) decreases when nitrites are incorporated and remains constant when phosphates are added. N_D increases with ageing time. These differences are interpreted in terms of the composition of each surface layer.

Introduction

It is widely accepted that the electronic properties of passive films correlate to the corrosion susceptibility of metals and alloys. For iron and iron-based alloys, several attempts to associate the protectiveness of the surface films to their electronic character have been published (1-5). It is quite established that the semiconducting properties of the passive films are associated to film breakdown and pit initiation (3). However, this relationship is far from being completely understood.

The context of the present investigation is the corrosion of construction steel. The first step in this type of investigation involves electrochemical studies in solutions that simulate the composition of the electrolyte that impregnates the pores of concrete, where chloride ions are key players in marine environments. In most cases, risky chloride concentrations build up after prolonged exposure times to fog and salty winds. However, chlorides can also be incorporated to the initial concrete mixture through the use of contaminated aggregates which frequently contain high levels of chlorides. To delay corrosion onset, inorganic inhibitors are frequently incorporated to concrete as corrosion inhibitors.

The passive film on carbon steel is generally regarded as a highly defective n type semiconductor, with a donor concentration of 10^{20}–10^{21} cm^{-3} (6). Azumi et al. (7) evaluated the passive films on iron in neutral borate and phosphate solutions showing that the carrier density and flat band potential depended on the ions present in the solution: phosphate but not borate ions, can penetrate into the passive film producing structural and electronic defects. Williamson et al. modeled the electronic properties of the passive films on carbon

steel in simulated concrete pore solutions with and without sulfate ions, changing the pH and using various passivation times (8). Their model, based on the presence of two discrete donor bands, accurately predicts experimental measurements. In a more recent publication, Williamson and Isgor (5) included the effect of chloride ion into the model. However, chlorides were added after pre-passivating the samples during 10 days in chloride-free solutions.

The passive film formed on iron and iron-based alloys is strongly dependent on how it grows (solution, time, potential, and other variables) which may explain some of the discrepancies between the results reported by different authors. Furthermore, although many studies have been devoted to analyze the film electrical properties, the interaction between the passive film and the ions that influence the corrosion process have rarely been reported. In this work, films are grown at open circuit potential in alkaline solutions containing chlorides. The electrical properties and film composition are studied, comparing electrodes aged in solutions with and without nitrite or phosphate ions as inhibiting agent.

Materials and methods

Electrodes and electrolyte

The electrodes were made out of steel reinforcement bars cut into discs. The average composition of the steel employed is: Mn 0.635 wt%, C 0.299 wt%, Si 0.258 wt%, Cu 0.227 wt% and others impurities 0.245 wt%. Fast curing epoxy resin was used to hold the discs into polyvinyl chloride (PVC) tubes. The geometrical area exposed resulted to be 0.50 cm^2. The electrodes were abraded down to grade 1000 using emery paper.

A pore simulating solution (Cl-PSS) was prepared by dissolving KOH 0.08 mol dm^{-3}, NaOH 0.02 mol dm^{-3}, $Ca(OH)_2$ 0.001 mol dm^{-3} (pH = 13). To analyze chloride contamination, NaCl 0.3 mol dm^{-3} was incorporated ($[Cl^-]/[OH^-]=3$). Na_3PO_4 and $NaNO_2$ were also added to analyze the effect of nitrites and phosphates as corrosion inhibitors. The dosage tested was 0.3 mol dm^{-3} in both cases, corresponding to $[inhibitor]/[Cl^-]=1$. These solutions will be referred to as Cl-PSS-phosphate or Cl-PSS-nitrite. All the experiments were carried out at room temperature (20 ± 2 ºC).

Electrochemical methods

For the electrochemical evaluation, a Pt counter-electrode, a Hg/HgO reference electrode with 1 mol dm^{-3} KOH solution (MOE, E = 0.123 V vs. SHE) were employed. All the potentials are shown against this reference.

The open circuit potential (OCP) was measured during 24 h in the different conditions investigated. Average values of at least five individual experiments were registered.

Electrochemical impedance spectroscopy (EIS) tests were performed at OCP on electrodes aged for 24 h and 7 days. The amplitude of the AC signal was ± 0.01 V_{rms} and the frequency varied between 20 kHz and 5 mHz.

The Mott–Schottky plots were obtained by imposing a fixed frequency of 1 kHz and using an excitation voltage of ± 0.01 V_{rms} with a scan rate of 50 mV/s.

The experiments were carried out using a Gamry CSM 100 and a Solartron 1280B Electrochemical Measurement Unit.

X-Ray Photoelectron Spectroscopy (XPS)

For XPS analysis, the samples were aged during 7 days at OCP. The XPS spectra were obtained as reported previously (9), using a XPS VG Microtech ESCA3000 (MgKα and AlKα radiations). The operating pressure was set at $3 \cdot 10^{-10}$ mbar and the incidence angle at 45º. Survey spectra were recorded within 0–1100 eV. Surface charging effects were compensated using the binding energy (BE) of the C 1s line of residual carbon as reference (284.5 eV BE) [19]. The spectra were analyzed using XPSPEAK41 software.

Results

Nitrites and phosphate ions are both excellent corrosion inhibition agents over long periods of times. The performance of these inhibitors was evaluated after 90 days immersion in OCP by carrying out weight-loss tests (10, 11). Steel coupons were immersed in PSS-Cl, PSS-Cl-nitrite and PSS-Cl-phosphate. The percentage of inhibition can be calculated as

$$\%\zeta = \left[1 - \frac{i_{\text{corr with inhibitor}}}{i_{\text{corr without inhibitor}}}\right] x100 \qquad [1]$$

The corrosion current density (i_{corr}) was calculated from weight loss results as i_{corr} = m F / (A t eq) (12), where m is the mass lost, F is the Faraday constant, A is the exposed area, t is the exposure time and eq is the equivalent weight (Fe eq= 27.92 g/mol).

The results are shown in Table 1. Photographs of the coupons after 90 days of immersion in each electrolyte can be seen elsewhere (10, 11). No attack was detected on the specimens immersed in the solutions containing either nitrites or phosphates, in spite of the presence of chloride ions. The inhibition efficiency attained values higher than 99%. In contrast, pitting is evident in the case of coupons immersed in PSS-Cl. Chloride ions promote passivity breakdown of steel as a result of the competition of two processes: OH^- and Cl^- adsorption. When the activity of chlorides overcomes that of hydroxyls, pitting occurs (13).

TABLE I. Weight loss results after 90 days of immersion at OCP in the different solutions tested

Condition	Type of attack	Weight loss / mg	% Inhibition
Cl-PSS	**Pitting**	**221.2**	**----**
Cl-PSS-nitrite	**None**	**0.1**	**99.99**
Cl-PSS-phosphate	**None**	**0.3**	**99.86**

Pitting investigation can be accelerated by recording anodic polarization curves. Some relevant electrochemical parameters such as passivity current density (i_{pas}), corrosion potential (E_{corr}) and pitting potentials (E_{pit}) were calculated from at least six anodic

polarization curves. These average results are presented in Table 2. As shown before in the presence of chloride ions (10), pitting occurs at potentials around 0 V_{MOE} and repassivation is not possible. When nitrites were incorporated to the chloride-contaminated solution, the pitting potential moved further away from the OCP. The corrosion current density (i_{pas}) measured in presence of nitrite ions is close to the value measured for non-contaminated PSS, and in Cl-PSS is over 3 times higher (10). These results are consistent with the fact that no pitting was observed after 90 days of immersion at the OCP, and clearly shows that nitrites behave as effective inhibitors. In contrast, when both phosphates and chloride ions are present in solution (9, 11), no pitting is observed by polarizing the electrode. The inhibition efficiency observed over long immersions periods is similar to that found for nitrites and the passivity current density decreases even more.

TABLE II. Relevant electrochemical parameters derived from polarization curves (10, 11).

	E_{corr} 24 h / mV_{MOE}	E_{pit} / mV_{MOE}	i_{pas}/ µA cm^{-2}
Cl-PSS	-229 ± 51	6 ± 64	5.4 ± 2.6
Cl-PSS-nitrite	-268 ± 90	658 ± 55	1.7 ± 1.1
Cl-PSS-phosphate	-279 ± 77	-----	0.9 ± 0.7

Impedance spectra were recorded using electrodes aged during 24 hours and 7 days in the electrolytes of interest. The results were fitted to the equivalent circuits presented in Figure 1 using ZView™ (14). Constant phase elements (CPE) can be described as:

$$Z_{CPE} = [Q(j\omega)^n]^{-1} \qquad [2]$$

where Q is a constant with dimensions of Ω cm^2 $s^{-(1-n)}$ and n a constant power, with -1<n<1. Warburg impedances and CPEs where n is close to 0.5 are used to model surface layers with high ionic conductivity. If the surface layer is thin, low frequencies will penetrate the entire thickness creating a finite length Warburg element (Eq.3):

$$Zw = \frac{W_R}{(iT\omega)^n}\tanh(iT\omega)^n \qquad [3]$$

where W_R is a parameter associated with diffusion processes, T is related to the effective diffusion coefficient (D) and the effective diffusion thickness (L) by $T = L^2/D$.

The results and the fitting curves are shown in Figure 2 and 3 (Bode plots). In all the conditions tested the high frequency time constant can be associated to the presence of a passive layer. At frequency lower than 10 Hz, one or two time constants could be associated to the charge transference resistance or diffusion process (13, 15,16). The fitting parameters are presented in Table 3. R_s represents the solution resistance, Q_o the pseudo-capacitance of the surface film, R_o the film resistance, Q_t the metal pseudo-capacitance, R_t the charge-transfer resistance for metal dissolution and and W_R represents a Warburg element associated to finite length diffusion through in the film. The experimental data fit reasonably well to the circuit proposed in Figure 1a, except for those experiments in Cl-PSS-phosphate, and Cl-PSS-nitrite after 7 days which fit to circuit in Figure 1b.

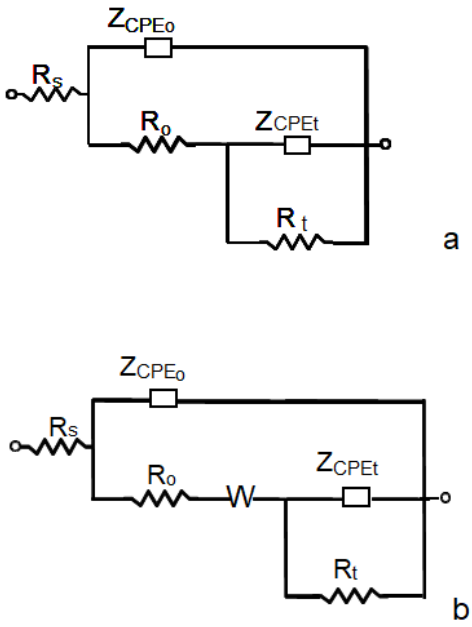

Figure 1. Equivalent circuits used to fit EIS results. Circuit a is typical of oxide-coated metals; circuit b presents an additional Warburg element, typical of situations where diffusion processes are involved.

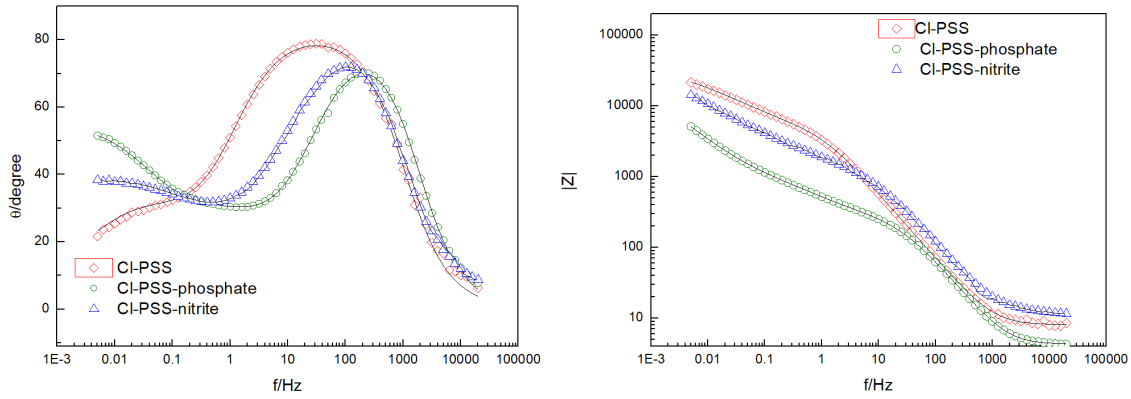

Figure 2. Impedance spectra (Bode representation) recorded on steel electrodes aged during 24 hours at OCP. The symbols represent the data and the lines the fitting results.

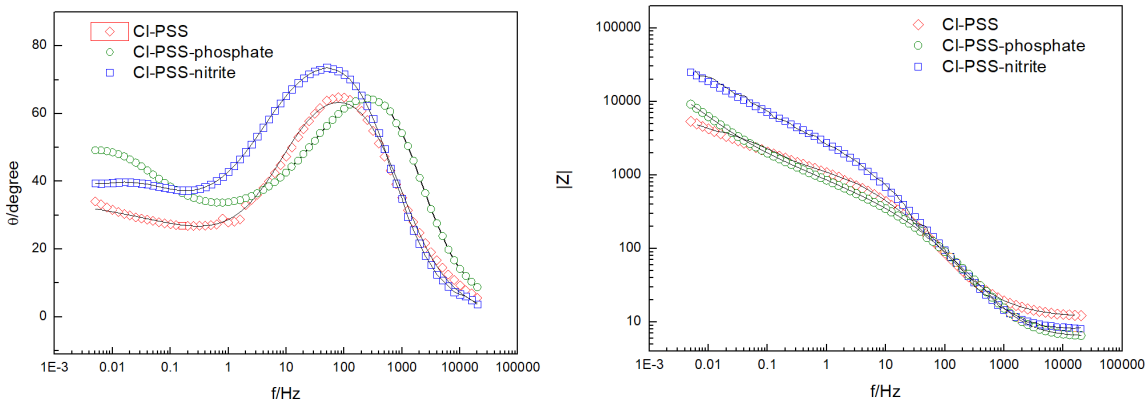

Figure 3. Impedance spectra (Bode representation) recorded on steel electrodes aged during 7 days at OCP. The symbols represent the data and the lines the fitting results.

TABLE III. Relevant parameters derived after fitting EIS results shown in Figures 2 and 3 to the equivalent circuits presented in Figure 1.

	Cl-PSS 24 h	**Cl-PSS 7 d**	**Cl-PSS-phosphate 24 h**	**Cl-PSS-phosphate 7 d**	**Cl-PSS-nitrite 24 h**	**Cl-PSS-nitrite 7 d**
$R_s/\Omega\ cm^2$	8.0	12.4	4.3	3.2	5.9	6.6
$Q_o/\mu\Omega^{-1}\ cm^{-2}\ s^n$	38.2	47.4	34.4	57.0	49.4	63.7
n_o	0.92	0.85	0.95	0.90	0.90	0.91
$R_o/\Omega\ cm^2$	4910	669	180	62	611	684
$W_R/k\Omega\ cm^2$	----------	----------	0.57	0.43	----------	7.43
T/s	----------	----------	1.81	0.77	----------	73.8
n_W	----------	----------	0.32	0.27	----------	0.35
$Q_t/\mu\Omega^{-1}\ cm^{-2}\ s^n$	232.9	725.1	2141	1955	742	1571
n_t	0.60	0.42	0.67	0.63	0.48	0.66
$R_t/k\Omega\ cm^2$	34.7	16.1	101.0	64.4	119.5	$>10^{20}$
X-square	0.0026	0.001	0.0001	0.0001	0.0009	0.0001

When only chloride ions are present in the electrolyte, the film becomes more porous and less protective at longer exposure times. Consequently, n_o, R_o and R_t decrease (17) and the corrosion current increases, as expected. Values of n_o higher than 0.9 can be related to a capacitive response associated to the presence of a protective passive layer (13, 15, 18, 19). Also, lower R_o values can be related to the presence of a more conductive passive layer, and not necessarily to a more defective or porous one (11, 19, 20).

For electrodes aged 24 h, the addition of nitrite or phosphate ions results in an increment in R_t, when compared to Cl-PSS. For the 7 days immersion period, R_o shows no significant difference when nitrites ions are present. However, R_t increases markedly to values higher than 10^{20}. This behavior could be attributed to the presence of a passive bilayer, where the inner layer is highly compact and protective, blocking metal dissolution (21). The decrease of R_o when phosphates are present during the 7 days ageing is probably related to changes in the composition which impact the electronic properties (11). Also, the diffusion impedance could be associated to a more difficult movement of cation vacancies.

These vacancies are generated by chloride ions adsorption and diffuse from the film/solution interface across the film, towards the film/metal interface.

Changes in the film properties can be confirmed evaluating their composition with XPS. Table 4 summarizes an analysis of the signal from films prepared by 7-day immersions in the three electrolytes. As it can been, the film in Cl-PSS is dominated by Fe(III) species with a small contribution from Fe^0, while in Cl-PSS-nitrite, the contents of Fe(II) and Fe(III) species are roughly half of each and the film grown in Cl-PSS-phosphate is rich in Fe(II). In Cl-PSS-nitrite there is no need to involve a Fe^0 peak, suggesting this is the thicker film, given that the thickness of the surface film exceeds 10 nm (which is the maximum depth that can be evaluated by XPS) (19).

TABLE IV. Characteristic parameters associated to the elements present on the surface film

Electrolyte	Signal	Origin	Binding energy/eV	FWHM/eV	Composition % at
Cl-PSS	Fe2p	Fe^0	706.7	1.3	3.1
		Fe(II)	709.6	1.3	1.2
		Fe(III)	711	4.5	95.7
	O1s	O^{-2}	530	1.7	79.7
		OH^-	531	1.4	20.3
Cl-PSS-nitrite	Fe2p	Fe^0	706.7	--	0
		Fe(II)	709.6	2.5	55.2
		Fe(III)	711	2.0	44.8
	O1s	O^{-2}	530	2.2	49.4
		OH^-	531	1.2	50.6
Cl-PSS-phosphate	Fe2p	Fe^0	706.7	1.5	9.5
		Fe(II)	709.6	2.9	67.0
		Fe(III)	711	2.5	23.5
	O1s	O^{-2}	530	0.6	9.3
		OH^-	531	1.1	47.3
		PO_4^{3-}	532	1.7	43.4

Table 5 shows Fe^{III}/Fe^{II} and Fe^{OX}/Fe^0 ratios, calculated from the analysis of XPS peaks. Fe^{OX} is calculated as the contribution from Fe(II) and Fe(III) peaks in Table 2 (18). Fe^{OX}/Fe^0 can be taken as the amount of Fe(II) and Fe(III) oxides formed, relative to the

quantity of metallic iron, Fe^0. The Fe^{OX}/Fe^0 ratios are very different and suggest that the composition and thickness of the corrosion products changes in the presence of nitrite or phosphate ions. The higher contribution of Fe(II) compounds in the passive film when the inhibitors are present can be associated to the improved corrosion resistance. As regards the O1s peak, the participation of hydroxides seems to increase when the inhibitor is added.

TABLE V. Fe^{III}/Fe^{II} and Fe^{OX}/Fe^0 ratios, calculated from the analysis of XPS peaks (see TABLE IV).

Condition	Fe^{III}/Fe^{II}	Fe^{OX}/Fe^0	d_{ox}(nm)
Cl-PSS	79.75	31.25	7.6
Cl-PSS-phosphate	0.35	9.52	5.1
Cl-PSS-nitrite	0.81	High	>10

The Fe^{OX}/Fe^0 ratio could be used to calculate the film oxide thickness assuming a uniform iron oxide layer present on the entire surface. Accordingly, the thickness of the surface film (d_{ox}) can be calculated as (22):

$$d_{ox} = \lambda_{ox}^{Fe} \cos\theta \ \ln\left(1 + \frac{I_{ox}^{Fe}}{I_M^{Fe}} \cdot \frac{N_M^{Fe}}{N_{ox}^{Fe}} \cdot \frac{\lambda_M^{Fe}}{\lambda_{ox}^{Fe}}\right) \quad [4]$$

where ɵ is the refracted angle to the normal surface; and I_{ox}^{Fe} and I_M^{Fe} correspond to the intensity of the peaks related to oxides and to iron, respectively. N_M^{Fe} and N_{ox}^{Fe} are atom densities of iron oxide and metallic iron (N_M^{Fe}= 84 atom/nm^3 and N_{ox}^{Fe}= 38 atom/nm^3 respectively). In turn, λ_M^{Fe} and λ_{ox}^{Fe} are the attenuation lengths of iron oxide and iron, which can be calculated as (22):

$$\lambda_{ox}^{Fe} = 0.72\ (a_{ox})^{3/2}(E_k)^{1/2} \quad [5]$$

$$\lambda_M^{Fe} = 0.41\ (a_M)^{3/2}(E_k)^{1/2} \quad [6]$$

where E_k (eV) is the kinetic energy of iron (779 eV); a_{ox} and a_M (nm) are the monolayer thicknesses of iron oxide and metallic iron, respectively

$$a_{ox} = \left(\frac{1}{N_{ox}^{Fe}}\right)^{1/3} \quad [7]$$

$$a_M = \left(\frac{1}{N_M^{Fe}}\right)^{1/3} \quad [8]$$

Using eqns. 4-8, the oxide film thicknesses was calculated for Cl-PSS and Cl-PSS-phosphate. The results are presented in Table 5. The film thickness increases when nitrite ions are present and decreases in the case of phosphate.

Mott–Schottky tests were conducted to explore the effect of nitrite and phosphate ions on the electronic properties of the passive films. The capacitance, C, can be obtained from C =1/ωZ", where ω is the angular frequency and Z" is the imaginary part of impedance.

Assuming as negligible the capacitance of the Helmhotlz layer, the capacitance C can be taken as equal to the space charge capacitance (C_{sc}), which is given by Eq. [9] (23),

$$\frac{1}{C^2} = \frac{2}{\epsilon\epsilon_0 e N_D}\left(E - E_{fb} - \frac{k_B T}{e}\right) \quad [9]$$

where ε is the dielectric constant of the film, ε_0 the vacuum permittivity, e the charge of an electron, N_D represents the donor concentration in the passive film, k the Boltzmann constant, V the applied potential, and V_{fb} the flat band potential. When applied to an n-type semiconductor, the equation results in a plot of C^{-2} versus V that should be linear, showing a positive slope that is inversely proportional to the donor concentration. The measured capacitance value can be influenced by the frequency, which for this system has been fixed at 1000 Hz (2, 24).

Figure 4 shows the effect of phosphate and nitrite ions on the Mott–Schottky plots for the passive films grown on construction steel held for 24 h and 7 days at OCP. The stability of films during MS tests was evaluated by measuring the capacitances in both forward and reverse scan directions. Only a very small hysteresis was observed within the potential window used in these tests.

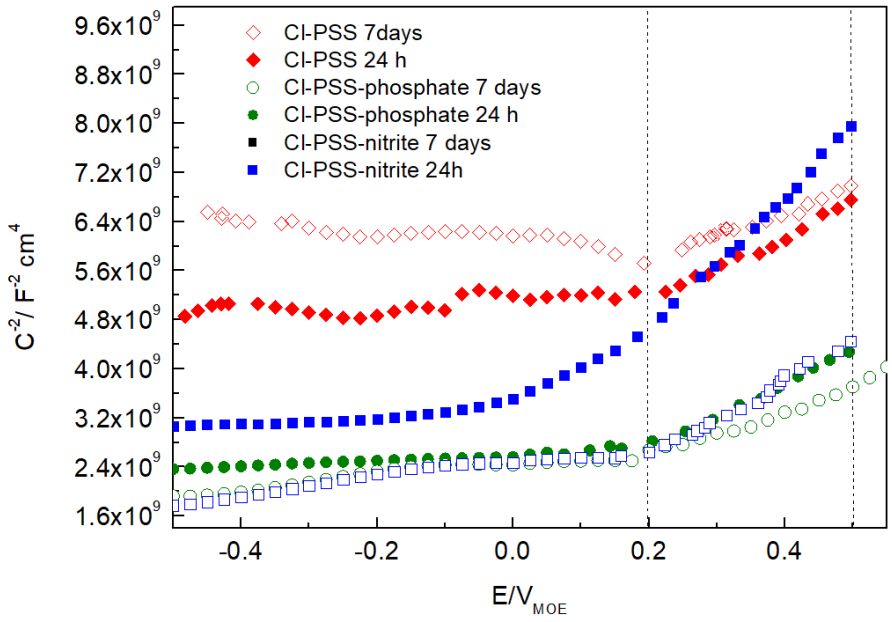

Figure 4. Mott-Schottky plots of films formed 24 h and 7 days at OCP in Cl-PSS, Cl-PSS-nitrite and Cl-PSS-phosphate.

The slope confirms the presence of n-type semiconductors. The donor concentration, calculated from the slope of linear part of the Mott–Schottky and taking ε = 12 (2, 5, 8) is summarized in Table 6. The Mott-Schottky plots recorded in these highly alkaline solutions have been modeled acknowledging the existence of two donor levels in the space charge layer (3, 5, 8). At high potentials, both the shallow and the deep levels of donor states

contribute to the electrode capacitance. Dashed lines in Figure 3 limit the zone were N_D values were obtained (0.2 to 0.5 V).

TABLE VI. Correlation between donor density (from eqn. 8) and pitting potential (6).

pH=13	E_{pit} / mV	Nd / cm^{-3} x 10^{-20} 24 h	Nd / cm^{-3} x 10^{-20} 7d
Cl-PSS	6 ± 64	19.6 ± 2.7	27.6 ± 5.1
Cl-PSS-nitrite	658 ± 55	12.1 ± 1.5	15.4 ± 3.2
Cl-PSS-phosphate	-----	20.1 ± 2.4	33.3 ± 4.5

As shown above, the presence of nitrites or phosphate ions during the ageing period yield inhibition efficiencies higher than 99%, even when chloride ions are simultaneously present. However, the effect of adding these inhibiting agents (either phosphates or nitrites) to the donor density values is not as clear. The results in Table 6 indicate that the donor density decreases when nitrites are incorporated to PSS-Cl. It has been established that the dopants in the passive film on carbon steel are mainly oxygen vacancies (24). Also, these and other authors have proposed that donor positions within the passive film are potential sites of film breakdown and pitting initiation. Our results for Cl-PSS-nitrite are also in agreement with those of Li et al. (25), who found that the pitting susceptibility of the passive film on iron improved as the donor concentration in the passive film decreased. In contrast, N_D shows only a slight increment when films grown in Cl-PSS-phosphate are compared to Cl-PSS. This can be interpreted taking into account the change in composition observed with XPS (more Fe(II)) and a thinner and more compact film that incorporates phosphates, where P atoms can act as donors.

Discussion

Nitrite and phosphate ions are known to inhibit steel corrosion in alkaline environments. In Cl-PSS-nitrite, the passive film is more protective than in the more aggressive condition (Cl-PSS), reaching the behavior of a blocking electrode with R_t values in the order of 10^{20}. As impedance and XPS results suggested, the presence of nitrite ions favors the development of a thick and protective passive layer rich in Fe(II) compounds (13). When steel is aged in contact with Cl-PSS-phosphate a ferrous phosphate layer forms by a dissolution-precipitation mechanism. Underneath this ferrous phosphate layer, a protective film of Fe_3O_4 could be formed via solid-state process (11, 19). Ferrous phosphate could be oxidized to ferric phosphate by reaction with oxygen (26). After long periods of time at OCP, the ferric phosphate layer could inhibit Fe_3O_4 oxidation, avoiding attack by chloride ions. In addition, this phosphate layer could delay oxygen diffusion through the duplex interface, hindering the consumption of the electrons produced by the anodic reaction taking place at the metal-film interface (27, 28). Instead, in inhibitor-free Cl-PSS the detrimental effect of chloride ions is evident, producing a more porous and less protective surface layer, rich in Fe(III).

It has been generally accepted that lower donor densities translate into lower susceptibility of the passive film to pitting corrosion. Cheng et al. (24) have proposed that donor positions within the passive film are potential sites of film breakdown and pitting initiation. Ahn et al. (2) found that as the concentration of Fe^{2+} ions in the film increases, the more susceptible is the passive film is to pitting, given that Fe^{+2} ions can also act as donors. This finding is in disagreement with our results. Our results in Cl-PSS-nitrite are in line with those of Li et al. (25), who found that the pitting susceptibility of the passive film on iron improved as the donor concentration in the passive film decreased. The higher Fe(III) concentration in the passive layer on carbon steel at pH=13 contaminated with chloride ions could be responsible of an increment of N_D (more deep donors associated to this disordered structure) (8). However, films aged in Cl-PSS-phosphate incorporate phosphates, and the donor density shows no significant changes when compared to Cl-PSS even when the surface film can prevent localized corrosion.

In summary, while it is generally accepted that the increment in the donor density enhances the susceptibility of the passive film to pitting corrosion, our results demonstrate that this is not always the case. The donor density does not decrease when an effective inorganic inhibitor such as phosphate ions is present, showing that this parameter cannot be taken as a direct proof for corrosion risk. The results must be interpreted in terms of the composition of the surface film.

Conclusions

The performance of nitrite and phosphate ions as corrosion inhibitors has been evaluated in simulating solutions contaminated with chloride ions. Over long periods of time, both show inhibition efficiencies higher than 99%.

Electrochemical impedance spectroscopy and XPS results demonstrate that the surface film that develops on steel changes significantly when the contaminant and the inhibiting agent are present simultaneously. In Cl-PSS, a duplex surface layer is formed at OCP with an inner layer of Fe_3O_4 and more defective outer layer mostly composed of FeOOH and presenting higher number of oxygen vacancies.

When the surface film develops in contact with nitrite ions, the Fe^{3+}/Fe^{2+} ratio decreases and the film becomes thicker and more protective, which is accompanied by a decrease in the donor density values.

When the passive film grows in contact with phosphate ions the $Fe^{3+/}Fe^{2+}$ ratio decreases even more, while the donor density values show a very slight increase. This film consists of an outer layer of ferrous phosphate progressively oxidized to ferric phosphate, and an inner, protective layer of Fe_3O_4 formed via solid-state process.

In every case, as the surface layers grow over longer periods of time, the ageing is accompanied by an increment in the donor density values, probably associated to a higher degree of disorder.

Acknowledgements

The authors have received financial support from the University of Mar del Plata (Grant 15/G450), as well as by the National Research Council (CONICET, PIP0670), Argentina.

The authors are indebted to Dr. Wido Schreiner, from Universidade Federal do Paraná, Brazil, for his help with XPS analysis.

References

1 . C. Y.F. and L. J.L., Electrochimica Acta **44** 2947-2957 (1999).
2 . S.J. Ahn and H.S. Kwon, Electrochimica Acta **49** 3347-3353 (2004).
3 . Y.F. Cheng and J.L. Luo, Electrochimica Acta **44** 2947±2957 (1999).
4 . S.P. Harrington, F. Wang and T.M. Devine, Electrochimica Acta **55** 4092-4102 (2010).
5 . J. Williamson and O.B. Isgor, Corrosion Science 106 82-95 (2016).
6 . D.G. Li, Y.R. Feng, Z.Q. Bai, J.W. Zhu and M.S. Zheng, Electrochimica Acta 52 7877-7884 (2007).
7 . K. Azumi, T. Ohtsuka and N. Sato, J Electrochem Soc 134 1552-1357 (1987).
8 . J. Williamson, V.J. Asad and O.B. Isgor, J Electrochem Soc 162 C619-C629 (2015).
9 . L. Yohai, W. Schreiner, M. Vázquez and M.B. Valcarce, Electrochimica Acta 202 231-242 (2016).
10. S. Toujas, M. Vazquez and M.B. Valcarce, Corrosion Science in press (2017).
11. L. Yohai, M. Vázquez and M.B. Valcarce, Electrochimica Acta 102 88-96 (2013).
12. American Society of Testing and Materials, ASTM G102-89, Philadelphia, 1994.
13. M.B. Valcarce and M. Vázquez, Electrochimica Acta 53 5007-5015 (2008).
14. ZPlot for Windows Scribner Associates Inc.1998.
15. M.B. Valcarce, C. López and M. Vázquez, J Electrochem Soc 159 C244 (2012).
16. M.B. Valcarce and M. Vázquez, Mater Chem Phys 115 313-321 (2009).
17. L. Hamadou, A. Kadri and N. Benbrahim, Appl Surf Sci 252 1510-1519 (2005).
18. P. Ghods, O.B. Isgor, J.R. Brown, F. Bensebaa and D. Kingston, Appl Surf Sci 257 4669-4677 (2011).
19. W. Xu, K. Daub, X. Zhang, J.J. Noel, D.W. Shoesmith and J.C. Wren, Electrochimica Acta 54 5727-5738 (2009).
20. C. Liu, Q. Bi, A. Leyland and A. Matthews, Corrosion Science 45 1243-1256 (2003).
21. M. E. Orazem and B. Tribollet, Electrochemical Impedance Spectroscopy, John Wiley & Sons (2008).
22. M. P. Seah and W.A. Dench, Surf Interface Anal 1 2-11 (1979).
23. J.F. Dewald, J Phys Chem Solids 14 155 (1960).
24. S. Schorr, Solar Energy Materials and Solar Cells 95 1482-1488 (2011).
25. W. Li and J. Luo, Electrochemistry Communications 1 349–353 (1999).
26. S. I.V., H. Hildebrand, S. Virtanem and P. Schmuki, Corrosion Science 48 3472-3488 (2006).
27. M. Sancy, Y. Gourbeyre, E.M.M. Sutter and B. Tribollet, Corrosion Science 52 1222-1227 (2010).

28. D.A. Jones, Principles and prevention of corrosion-2nd, Prentice-Hall Inc. (1996).